EES Catalysis

PAPER

View Article Online
View Journal | View Issue

Cite this: *EES Catal.*, 2025, 3, 783

Two-step tandem electrochemical conversion of oxalic acid and nitrate to glycine†

Yuan-Zi Xu, Daniel F. Abbott, Lok Nga Poon and Victor Mougel *

Received 20th January 2025,
Accepted 30th March 2025

DOI: 10.1039/d5ey00016e

rsc.li/eescatalysis

This study presents a facile tandem strategy for improving the efficiency of glycine electrosynthesis from oxalic acid and nitrate. In this tandem electrocatalytic process, oxalic acid is first reduced to glyoxylic acid, while nitrate is reduced to hydroxylamine. Subsequent coupling of these two precursors results in the formation of a C–N bond, producing the intermediate glyoxylic acid oxime, which is further reduced *in situ* to glycine. Here we show, using only a simple Pb foil electrode, which maximizes the yield of the first step of the transformation (*i.e.* the reduction of oxalic acid to glyoxylic acid) prior to the coupling step allows for an unprecedented selectivity and conversion for glycine electrosynthesis to be achieved. Overall, a maximum glycine faradaic efficiency (FE) of 59% is achieved at -300 mA cm^{-2} and a high glycine partial current density of -232 mA cm^{-2} and a glycine production rate of 0.82 mmol h^{-1} cm^{-2} are attained at -400 mA cm^{-2}, thereby paving the way for an energy and economically efficient electrochemical synthesis of glycine.

Broader context

The global demand for glycine, a fundamental amino acid with applications in nutrition, cosmetics, and industrial processes, is growing. However, current production methods are based on energy-intensive, environmentally challenging chemical processes that rely on non-renewable resources. This work presents a novel two-step tandem electrochemical method for glycine synthesis, utilizing oxalic acid (a potential derivative of CO_2) and nitrate, offering a pathway toward sustainable amino acid production. By coupling electrochemical steps with an optimized reaction design, this approach significantly improves efficiency and selectivity, surpassing existing electrosynthetic routes and demonstrating promising scalability for industrial applications.

Introduction

Glycine is the simplest amino acid and is fundamental in protein synthesis. It plays a pivotal role in the central metabolic pathways and therefore has a variety of potential uses, such as an enhancer or in food additives, dietary supplements, and cosmetics.[1–4] Unlike more complex amino acids, glycine's industrial production relies on chemical synthesis, primarily involving the substitution reaction of chloroacetic acid with ammonia.[5–8] Nevertheless, despite its apparent simplicity, this process encounters several challenges, including high energy consumption, environmental pollution, substantial catalyst usage, and significant capital investment.[9–12] The pursuit of environmentally sustainable glycine production hence holds considerable economic and social significance. Electrocatalysis has emerged as a promising avenue for amino acid synthesis, offering the advantages of zero carbon emissions through renewable energy utilization and by leveraging substantial electrochemical research from other fields, such as CO_2 reduction and N_2 reduction.[13–19] In addition, analyzing thermodynamics to evaluate the compatibility of different reactions has emerged as a straightforward strategy to formulate tandem catalytic processes, which can potentially take advantage of the thermodynamic leveraging between the different reactions involved.[20–22] Furthermore, formulating tandem catalytic processes addresses the issue of low conversion rates of intermediates, which ultimately results in the diminished yield of target products.[23–25] Notably, this approach has not received much attention in the field of electrochemistry, despite the readily available thermodynamic and kinetic data.

Given the remarkable selectivity of the electroreductive amination of α-keto acids using hydroxylamine as the N-source, as was pioneered by the Yamauchi research group,[26,27] our investigation focuses on an assisted tandem approach for electro-synthesizing glycine from oxalic acid and nitrate. Oxalic acid, the simplest dicarboxylic acid, exhibits potential as a platform chemical owing to its feasible production from various renewable and sustainable

Department of Chemistry and Applied Biosciences, ETH Zürich, Vladimir-Prelog-Weg 1-5, 8093 Zürich, Switzerland. E-mail: mougel@inorg.chem.ethz.ch

† Electronic supplementary information (ESI) available. See DOI: https://doi.org/10.1039/d5ey00016e

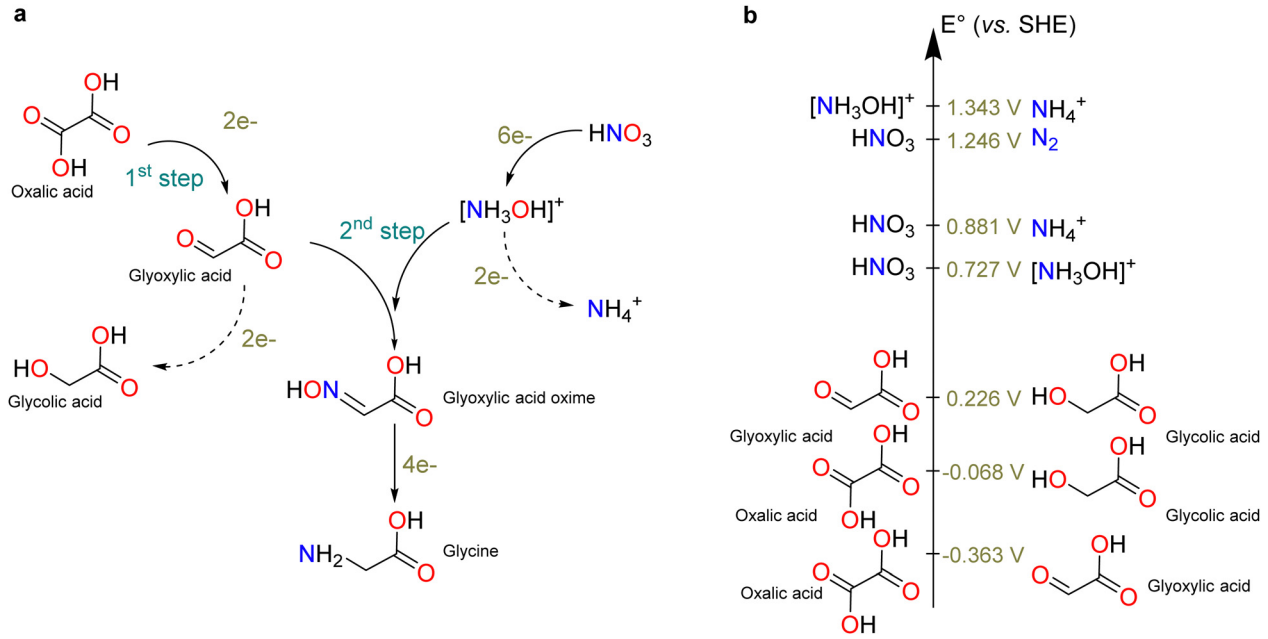

Scheme 1 Tandem strategy for the electrochemical conversion of oxalic acid and nitrate to glycine (a) and associated standard redox potentials (b).

feedstock sources, most notably from CO_2.[28–31] During the course of our work, two studies reported one-pot approaches for the electrochemical synthesis of glycine, utilizing oxalic acid and nitrate as starting materials, using a copper–mercury (Cu–Hg) electrode or Fe single atom on nitrogen-doped carbon materials.[32,33] While very promising, the modest partial current densities, around -100 mA cm^{-2} indicates potential for further optimization.

Achieving high selectivity in such a complex tandem catalytic reaction, however, is extremely challenging as it requires the balance of four main reactions: (1) the reduction of oxalic acid to glyoxylic acid, (2) the reduction of nitrate to hydroxylamine, (3) the coupling of this N-based synthon with glyoxylic acid, and finally (4) its reduction to glycine, as illustrated in Scheme 1a. One of the key impediments to higher efficiencies of tandem approaches appears to be the inherent chemical stability and low electrophilicity of the carboxylic carbons, owing to their location within a conjugated O–C–O system, thereby justifying the use of strongly acidic reaction media to facilitate the reduction of oxalic acid to glyoxylic acid.[34] Unfortunately, such an operation in highly acidic media has several drawbacks, in addition to posing challenges associated with the corrosion of the material, as it will inherently reduce the FE of the targeted tandem reaction. Indeed, strongly acidic conditions will also promote the further reduction of glyoxylic acid to glycolic acid, and the reduction of hydroxylamine to ammonia, as was observed at the highest current densities in previous studies.[32]

Achieving the tandem reduction in acidic media is further complicated by the fact that the standard reduction potential of oxalic acid to glyoxylic acid ($E = -0.363$ V – here and below in text, all potential are referenced *vs.* SHE unless otherwise specified) is over 1 V more cathodic than the standard reduction potential of nitric acid to hydroxylammonium (E = 0.727 V) or than that of nitric acid to ammonium (E = 0.881 V) (Scheme 1b and Tables S1, S2, Fig. S1, ESI†), which also contributes to the competitive direct reduction of the N-substrate and reduces the FE. Moreover, the more positive reduction potential of hydroxylamine to ammonium *versus* that of nitric acid to ammonium shows that it is prone to disproportionation. We reasoned that the presence of a large excess of glyoxylic acid in the media could therefore reduce the occurrence of this disproportion mechanism *via* the reaction of the generated hydroxylammonium with glyoxylic acid to generate the corresponding oxime and its subsequent reduction to glycine.

Building on the very extensive amount of work reporting on the reduction of oxalic acid to glyoxylic acid, which demonstrated that FEs and current densities competitive with existing industrial processes can be obtained using simple Pb, Hg, or graphite electrodes,[35–37] we propose in the present work an assisted, two-step tandem process to overcome the limitations of existing glycine electro-synthetic routes. Such a process requires a catalyst that would selectively mediate the four electrochemical reduction reactions of oxalic acid and nitrate to glycine, listed as (1)–(4) above, while being able to operate in acidic media to ensure efficient oxalic acid and glyoxylic acid oxime reduction steps. To mitigate competition with the hydrogen evolution reaction (HER) in such acidic media, and also considering the recognized performances of Pb electrodes for the reduction of oxalic acid to glyoxylic acid,[35–37] we investigated the use of Pb foil as an electrocatalyst to mediate these reactions. Moreover, to address the challenges arising from the lower onset potential for the reduction of nitrate *vs.* the reduction of oxalic acid, our strategy (Scheme 1a) involves the initial reduction of oxalic acid to glyoxylic acid, followed by the introduction of nitrate to the reaction mixture to facilitate its subsequent reduction, thereby coupling the electrogenerated hydroxylamine and the reduction of the oxime to generate glycine. Additionally, for simplified and cost-

effective product separation, we aimed to carry out the reaction in the absence of a supporting electrolyte. In the present case, we relied on using the substrates as both the reactants and the electrolyte, relying on the acidity of oxalic acid, glyoxylic acid, and glyoxylic acid oxime to be sufficient for mediating efficient coupling and reduction steps. A shift to higher pHs is then reached upon reaction completion when strong acids are no longer needed. Following these design guidelines, the individual optimization of the two steps of this tandem reaction enabled the realization of benchmark performances for the electrochemical glycine synthesis, reaching a FE of 59% at a high partial current density of -232 mA cm^{-2}.

Results and discussion

A simple Pb foil was chosen as the electrode material for conducting these investigations due to its high corrosion resistance in acidic media and high HER overpotential (see Fig. S2 for SEM/EDX characterization, ESI†).[38–40] As evidenced by the linear sweep voltammograms (LSVs) depicted in Fig. S3a (ESI†), the combined presence of oxalic acid and nitrate in solution results in higher catalytic currents between -0.45 V and -1.75 V than either reactant by itself. Preliminary studies, however, unexpectedly revealed that the use of sulfuric acid to maintain an acidic pH in the cathodic compartment had a detrimental effect on the catalytic activity (Fig. S3b, ESI†), resulting in the nearly exclusive production hydroxylamine, ammonia, and H_2. Therefore, subsequent experiments were carried out using only 0.5 M sodium nitrate and 0.5 M oxalic acid as the catholyte.

Fig. 1a presents the faradaic efficiency for each reaction product detected after 30 minutes of a one-pot, single-step electrolysis with applied current densities ranging from -50 to -600 mA cm^{-2} (see ESI,† and Fig. S4–S9 for quantitative details). In all cases, the FE for glycine during this single-step process remained under 15% and did not exhibit significant variation over time (Fig. S10, ESI†). However, analysis of the product distribution in these experiments underscores several critical aspects that need to be addressed in order to enhance the faradaic efficiency for glycine synthesis: (i) glyoxylic acid oxime is detectable across a broad range of current densities, suggesting that the condensation reaction between electrochemically generated glyoxylic acid and hydroxylamine occurs readily in the medium, (ii) at all current densities conducive to glycine formation, hydroxylamine emerges as the predominant product while glyoxylic acid oxime does not exceed 10%, which implies that the kinetics of nitrate reduction to hydroxylamine is significantly faster than the reduction of oxalic acid to glyoxylic acid, and (iii) this is consistent with the substantial detection of ammonia at all potentials, which indicates that the further reduction of hydroxylamine to ammonia is a

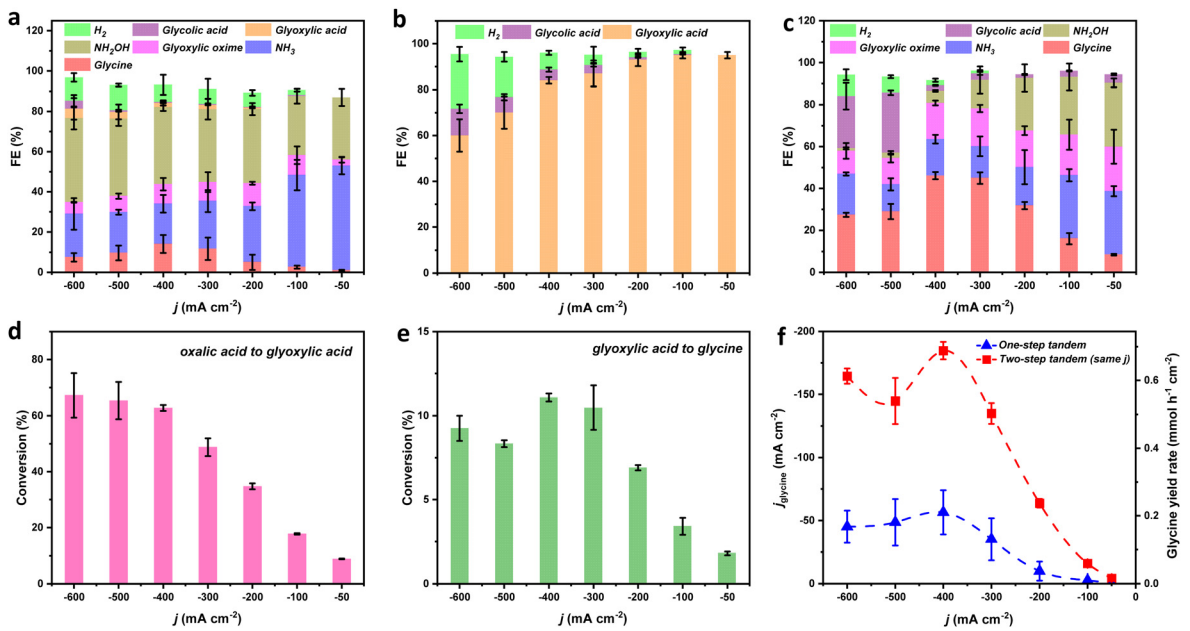

Fig. 1 (a) Faradaic efficiency of each product from the one-step tandem electrolysis in 0.5 M oxalic acid + 0.5 M $NaNO_3$ after 30 minutes at each current density. (b) Faradaic efficiency of each product from the oxalic acid to glyoxylic acid step (*i.e.* first step; in 0.5 M oxalic acid) after 30 minutes at each current density. (c) Faradaic efficiency of each product from the glyoxylic acid oxime to glycine step (*i.e.* second step; 0.5 M $NaNO_3$ added to the catholyte) after 30 minutes at each current density. (d) Corresponding conversion rates of oxalic acid to glyoxylic acid from the oxalic acid to glyoxylic acid electrolysis step. (e) Corresponding conversion rates of glyoxylic acid to glycine from the glyoxylic acid oxime to glycine electrolysis step. (f) Partial current densities and glycine generation rates after 30 minutes at each current density for the one-step tandem (blue curve) and two-step tandem (red curve) electrolysis methods (dotted lines are provided as a guide for the eye). The "one-step tandem" refers to a single-step electrolysis conducted in one pot using 0.5 M $NaNO_3$ + 0.5 M oxalic acid as the catholyte. The "two-step tandem (same *j*)" involves initially performing the oxalic acid to glyoxylic acid step in 0.5 M oxalic acid, followed by the addition of 0.5 M $NaNO_3$ to the electrolyte for glyoxylic acid oxime to glycine step. The two-step maintains the same current density (*j*) in both steps.

competitive pathway alongside its reaction with glyoxylic acid. These insights prompted us to transition from a single-step process to a two-step tandem strategy that facilitates the efficient initial reduction of oxalic acid to glyoxylic acid before introducing sodium nitrate to the medium.

To evaluate the efficacy of the two-step tandem strategy (see Experimental section and Fig. S11, ESI†) against the single-step approach, we initially conducted a 30-minute electrolysis step using the same setup as previously described, but in the presence of only 0.5 M oxalic acid as catholyte. After that first step, sodium nitrate was added to the catholyte solution to attain a concentration of 0.5 M and the electrolysis was pursued for another 30 minutes at the same current density (ranging from -50 to -600 mA cm^{-2}). Fig. S12 (ESI†) illustrates the corresponding steady-state polarization curves at various current densities for the two individual steps of the tandem process. Significantly higher applied potentials are required to achieve high current densities for the oxalic acid to glyoxylic acid step than are required for the glyoxylic acid oxime to glycine step, likely resulting from the increased conductivity of the electrolyte after addition of nitrate. The first step was found to be very effective for promoting the reduction of oxalic acid to glyoxylic acid, resulting in high FEs that decrease slightly upon increasing the current density, ranging from 95% at -50 mA cm^{-2} to 60% at -600 mA cm^{-2} for glyoxylic acid (Fig. 1b). This led to a 5- to 10-fold increase in the FE for glycine after the second step as compared to the single-step approach, reaching high FE for glycine of 45% at -300 mA cm^{-2} and 46.1% at -400 mA cm^{-2} (Fig. 1c). Both ammonia and hydroxylamine are present at all applied potentials, suggesting that both species could be involved in the C–N bond formation step. However, in agreement with previous studies,[27] we found that using ammonia instead of nitrate did not result in any glycine formation, while high yields were obtained using hydroxylamine (Fig. S13, ESI†).

Further analyzing the link between the two steps, we noted that the very high FE for glyoxylic acid in the first step observed at the lowest current densities does not translate into equally high FE for glycine in the second step. This is understandable given that the selectivity of the first step in such a tandem process has only a modest influence on the second step. In such a case, the selective conversion of oxalic acid to glyoxylic acid becomes a better descriptor (Fig. 1d). This is well exemplified here by the fact that at a low current density of -50 mA cm^{-2}, the selectivity for the reduction of oxalic acid to glyoxylic acid (first step) is close to unity (*i.e.* 100% FE; Fig. 1b), yet the selective conversion to glycine (second step) remains very low, reaching only around 2% (Fig. 1e). At such low current densities, glyoxylic acid, with its low production rate, becomes the limiting reactant when transitioning to the second step of the tandem system. Consequently, the excess hydroxylamine produced is further reduced to ammonia. As the current density increases in the first phase, however, the conversion from oxalic acid to glyoxylic acid gradually improves. This enhancement in conversion then comes at the expense of selectivity when it surpasses 60%; the over-reduction to glycolic acid is noticeable from -500 mA cm^{-2} and is accompanied by the emergence of increased quantities of H_2 (Fig. 1c), as was also observed in other studies.[28] Conversely, the production of hydroxylamine in the glyoxylic acid oxime to glycine step gradually decreases from -50 to -400 mA cm^{-2} and is accompanied by an increased amount of glycine formed. This highlights that glyoxylic acid remains the limiting reactant up to -400 mA cm^{-2}. At higher current densities, hydroxylamine now becomes the limiting reactant, being fully consumed in the coupling reaction with glyoxylic acid. This leads to the overreduction of the excess glyoxylic acid to glycolic acid above -500 mA cm^{-2} (Fig. 1c) and the parallel decline of $FE_{glycine}$. Related to the influence of current density on glyoxylic acid conversion (Fig. 1e, the conversion rate of oxalic acid to glycine is shown in Fig. S14, ESI†), a maximum of conversion is observed at -400 mA cm^{-2}, which corresponds to up to an 11% conversion after 30 minutes using the tandem electrolysis method. In our tandem approach, we observed notably higher partial currents for glycine compared to those achieved in a single-step process at identical applied current densities (Fig. 1f). Remarkably, without individually optimizing each step, the partial current density for glycine at an applied current density of -400 mA cm^{-2} reached -184 mA cm^{-2}. This level of performance suggests that our method could already be competitive with existing industrial processes for glycine synthesis.[27,41–43] However, the observation of a plateau in the partial current densities for glycine at and beyond -400 mA cm^{-2} highlights the potential for further enhancements through the independent optimization of each step in the process.

To investigate how reaction time affects product formation in the second step of the reaction, we conducted the glyoxylic acid oxime to glycine process at an applied current density of -200 mA cm^{-2} for an extended period of 3.5 hours (following 30 minutes of electrolysis for the oxalic acid to glyoxylic acid step at a fixed current density of -400 mA cm^{-2}). Following the FE of glycine over time (Fig. 2a), we observed that the $FE_{glycine}$ remained constant over the first 2 hours, but subsequently declined together with a significant increase of the FE_{H_2} and FE_{NH_3}. This trend is coupled with a decrease in FE_{NH_2OH} while $FE_{glycolic\ acid}$ continues increasing, suggesting that the reduction of nitrate is the limiting step after 2.5 hours. To circumvent that limitation, we attempted to modulate the molar concentration ratio of oxalic acid to nitrate from 2 : 1 to 1 : 2. However, as highlighted in Fig. 2b, equimolar concentrations of oxalic acid and nitrate gave the highest selectivity to glycine, preventing the undesired overreduction of the reactants to glycolic acid and ammonia, respectively. Further considering the evolution of product selectivity over time in Fig. 2a, we observed that HER starts increasing from 1.5 hours, whereas glycine selectivity only begins to decrease after >2 hours. This temporal discrepancy suggests that HER enhancement is not solely a consequence of reactant depletion, prompting us to investigate whether the concentration of sulfuric acid in the anolyte could influence HER in the cathode compartment. We could validate that the concentration of sulfuric acid in the anolyte indeed had an impact on the observed HER in the cathode compartment. As shown in Fig. 2c, a higher FE_{H_2} is observed upon increasing the H_2SO_4 concentration from 0.5 M to 1 M in the anolyte. However, decreasing the H_2SO_4 concentration to 0.1 M

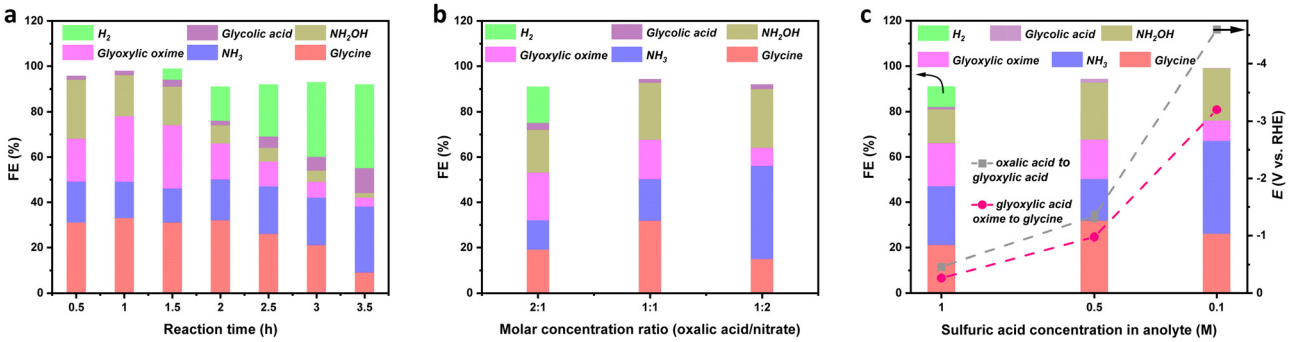

Fig. 2 (a) Faradaic efficiency of each product after the second step of the two-step tandem electrolysis (*i.e.* glyoxylic acid oxime to glycine step) at an applied current density of −200 mA cm^{-2} for an extended time of 3.5 h. (b) Corresponding changes in glycine faradaic efficiency under different molar concentration ratios of oxalate to nitrate after 30 minutes at an applied current density of −200 mA cm^{-2}. (c) Effect of the H_2SO_4 concentration in the anolyte on the FE and cell potential after 30 minutes at an applied current density of −200 mA cm^{-2}.

did not improve $FE_{glycine}$ and instead had a detrimental effect, resulting in a high cell resistance (Table S3, ESI†) and cell potential. The pH of catholytes was monitored during the tandem reduction process (Fig. S15, ESI†). Initially, oxalic acid (pH = 0.6) is reduced to glyoxylic acid, causing a rise in pH due to the higher pK_a of glyoxylic acid ($pK_{a,glyoxylic\ acid}$ = 3.13) compared to oxalic acid ($pK_{a,oxalic\ acid}$ = 1.25), making it less acidic. In the next step, glyoxylic acid oxime is reduced to glycine, which results in a slight pH increase, stabilizing around 1.6, even at −600 mA cm^{-2}. Despite the pH increase,

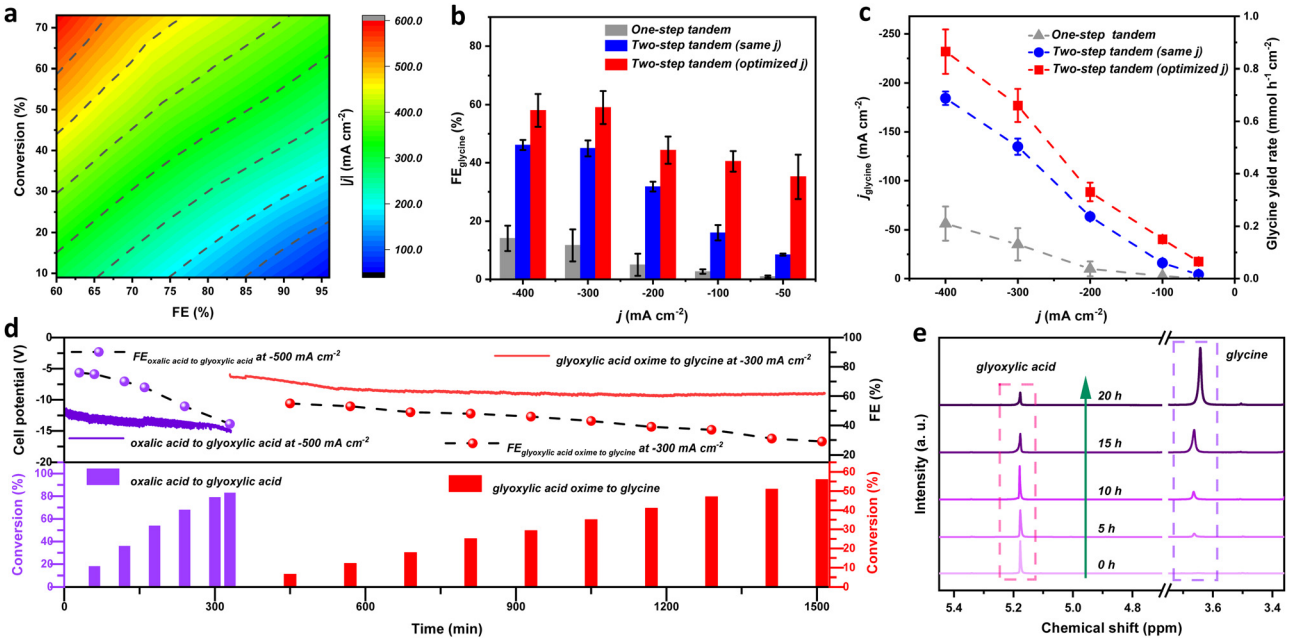

Fig. 3 (a) Mapping of the FE and conversion for the oxalic acid to glyoxylic acid step as a function of current density. The data were obtained from a 30-minute electrolysis step at different current densities in 0.5 M oxalic acid. (b) Faradaic efficiency of glycine at different current densities in the glyoxylic acid oxime to glycine step with the current density fixed at −500 mA cm^{-2} in the oxalic acid to glyoxylic acid step. The one-step tandem and two-step tandem electrolysis were plotted for comparison. (''One-step tandem'' refers to a single-step electrolysis conducted in one pot using a catholyte comprising 0.5 M $NaNO_3$ and 0.5 M oxalic acid. ''Two-step tandem (same *j*)'' involves initially performing the oxalic acid to glyoxylic acid step in 0.5 M oxalic acid, followed by the addition of 0.5 M $NaNO_3$ to the electrolyte for the glyoxylic acid oxime to glycine step. Both steps maintain the same current density. ''Two-step tandem (optimized *j*)'' follows a similar procedure to ''Two-step tandem (same *j*),'' but with the glyoxylic acid oxime to glycine step fixed at −500 mA cm^{-2}). (c) Partial current density and generation rate of glycine at different current densities in glyoxylic acid oxime to glycine step with the current density fixed at −500 mA cm^{-2} in the oxalic acid to glyoxylic acid step. The one-step tandem and two-step tandem electrolysis were plotted for comparison. (d) Voltage curves, conversion, and FE plots for long-term performance. Long-term performance tests were performed in a flow electrolytic cell using a constant applied current density of −500 mA cm^{-2} for 5.5 hours during the oxalic acid to glyoxylic acid step and at −300 mA cm^{-2} for 20 hours during the glyoxylic acid to glycine step. Dotted lines are provided as guides for the eye. (e) ^1H NMR spectra of glycine and glyoxylic acid as a function of time from the long-term performance tests of the glyoxylic acid oxime to glycine step. Note that glycine, due to its zwitterionic nature, exhibits a small concentration-dependent shift attributed to self-association, whereas glyoxylic acid, predominantly hydrated in solution, remains unchanged.

the environment remains sufficiently acidic to support the reaction and glycine formation, with the required acidic conditions maintained solely by the oxalic acid solution, enabling the tandem process without additional acidic reagents.

We hypothesized that the increased amounts of H_2 observed at long electrolysis time in the second step could also originate from the low pK_a of unconverted oxalic acid. Given the significantly higher pK_a of glyoxylic acid (p$K_{a,\text{oxalic acid}}$ = 1.25, p$K_{a,\text{glyoxylic acid}}$ = 3.13), we reasoned that increasing conversion in the first electrolysis step could help further enhance the selectivity. The performance of the first electrolysis step towards glyoxylic acid production was hence systematically assessed by FE, conversion rate, and current density over a 30 min electrolysis step to identify the optimal operating conditions for the oxalic acid to glyoxylic acid step (Fig. 3a). The highest selectivity was observed at low current densities (> -200 mA cm^{-2}), yet at the cost of low conversion rates (below 10%), while significantly higher conversion (over 70%) can be observed at high current densities (< -400 mA cm^{-2}). We found that an applied current density of -500 mA cm^{-2} allowed for the best compromise between high glyoxylic acid FEs (*ca.* 72%) and high oxalic acid conversion rates (over 75%) to be achieved. We reasoned that such a high conversion of oxalic acid would ensure the provision of an environment rich in glyoxylic acid for the subsequent step of the tandem reaction, thus further enhancing the performance of the tandem system. Indeed, a significant improvement of the $FE_{glycine}$ was then observed over a wide current density range (-50 to -400 mA cm^{-2}) when using these optimized conditions for the first step of the tandem process (Fig. 3b; Two-step tandem (optimized)). We observed a benchmark glycine FE of 59% when applying a current density of -300 mA cm^{-2}, while a very high glycine production rate of 0.82 mmol h^{-1} cm^{-2} was observed at a current density of -400 mA cm^{-2} (Fig. 3c). Not only are these performances far superior to the one-step method and the two-step tandem (same *j*) method for both steps introduced here, but this system also outperformed all previously reported systems in terms of $FE_{glycine}$, $j_{glycine}$, and glycine yield (Table S4, ESI†).[32,44–52]

Last, to investigate the applicability of our optimized two-step tandem glycine synthesis on a preparative scale, we translated this tandem strategy to an electrolyzer flow cell aimed at long-term electrolysis. In the first step, the continuous reduction of a 0.5 M oxalic acid solution (60 mL; recirculated) was conducted for 5.5 hours in a flow cell at a current density of -500 mA cm^{-2}, resulting in an overall selective conversion of oxalic acid to glyoxylic acid of 81% (Fig. 3d, purple line). Subsequently, sodium nitrate was introduced into the catholyte solution to achieve a concentration of 0.5 M NO_3^-, and electroreduction was pursued at an applied current density of -300 mA cm^{-2} for about 20 hours. The cell potential increased over time for both steps, accompanied by a decrease in the FE of both glyoxylic acid and glycine. This trend is likely attributable to the decreasing reactant concentration over time, which agrees with the increase in the selective conversion to both products. This was validated by the ^{1}H NMR monitoring of the second step of the tandem reaction, demonstrating a continuous decrease in glyoxylic acid concentration concomitant with an increase in glycine concentration (Fig. 3e). After 20 h, this resulted in a 56% conversion of glyoxylic acid to glycine (Table S5, ESI†), corresponding to over 1 g of electrosynthetized sodium glycinate. Post-characterization revealed surface roughening of the Pb foil after long-term testing, as observed in the SEM (Fig. S16, ESI†) and EDX (Fig. S17, ESI†) analysis.

Conclusions

This study demonstrates a two-step tandem strategy for electrochemical glycine synthesis, significantly improving faradaic efficiency and partial current density compared to one-step approaches. Beyond this specific case, this work highlights how simple redox potential considerations can guide the rational design of a tandem electrocatalytic process performing at industrially relevant reaction rates while maintaining high selectivity. We believe that this approach could be extended to other tandem electrochemical transformations, enabling the development of scalable electrosynthetic methodologies for precursors that are incompatible with single-step processes.

Author contributions

Y-Z. X. conducted the experiments with support from L. N. P., and D. A.; Y-Z. X., L. N. P. and V. M. analysed data; Y-Z. X. and V. M. wrote the manuscript with support from the all co-authors; Y-Z. X. and V. M. designed the research; and V. M. supervised the project.

Data availability

The data supporting the findings of this study have been included as part of the ESI.†

Conflicts of interest

There are no conflicts to declare.

Acknowledgements

Y-Z. X., D. A. and V. M. thank the European Research Council (ERC) under the European Union's Horizon 2020 research and innovation program (Grant Agreement No. 853064) for support. V. M. and L. N. P. acknowledge funding from the Swiss National Science Foundation (SNSF) project funding (Grant 200021_197153/1). Y.-Z. X. is grateful to the Chinese Scholarship Council for a fellowship.

References

1 K. Ivanov, A. Stoimenova, D. Obreshkova and L. Saso, *Biotechnol. Biotechnol. Equip.*, 2013, **27**, 3620–3626.
2 H. A. Abdulmumeen, A. N. Risikat and A. R. Sururah, *Int. J. Chem. Biochem. Sci.*, 2012, **1**, 36–47.

3 Y.-P. Xue, C.-H. Cao and Y.-G. Zheng, *Chem. Soc. Rev.*, 2018, **47**, 1516–1561.
4 J. F. Hyslop, S. L. Lovelock, P. W. Sutton, K. K. Brown, A. J. Watson and G. D. Roiban, *Angew. Chem., Int. Ed.*, 2018, **130**, 14017–14020.
5 S. Kinoshita, *Adv. Appl. Microbiol.*, Elsevier, 1959, vol. 1, pp. 201–214.
6 M. S. Dunn and L. B. Rockland, *Adv. Protein Chem. Struct. Biol.*, Elsevier, 1947, vol. 3, pp. 295–382.
7 L. M. Yang, N. N. Jiang and Z. Y. Zhao, *Adv. Mat. Res*, 2012, **396**, 1711–1715.
8 M. S. Dunn, A. Butler and E. H. Frieden, *J. Phys. Chem.*, 1941, **45**, 1123–1137.
9 H. Zhao, R. Yu, H. Qiao and C. Liu, *ACS Omega*, 2020, **5**, 13463–13472.
10 J. Zhou, J. Li, R. An, H. Yuan and F. Yu, *J. Agric. Food Chem.*, 2012, **60**, 6279–6285.
11 G. Tzvetkov, G. Koller, Y. Zubavichus, O. Fuchs, M. Casu, C. Heske, E. Umbach, M. Grunze, M. Ramsey and F. Netzer, *Langmuir*, 2004, **20**, 10551–10559.
12 J. Wang, X. Liu and X. Feng, *Chem. Rev.*, 2011, **111**, 6947–6983.
13 D. Pletcher, *Electrochem. Commun.*, 2018, **88**, 1–4.
14 S. A. Akhade, N. Singh, O. Y. Gutiérrez, J. Lopez-Ruiz, H. Wang, J. D. Holladay, Y. Liu, A. Karkamkar, R. S. Weber and A. B. Padmaperuma, *Chem. Rev.*, 2020, **120**, 11370–11419.
15 S. Möhle, M. Zirbes, E. Rodrigo, T. Gieshoff, A. Wiebe and S. R. Waldvogel, *Angew. Chem., Int. Ed.*, 2018, **57**, 6018–6041.
16 C. A. Malapit, M. B. Prater, J. R. Cabrera-Pardo, M. Li, T. D. Pham, T. P. McFadden, S. Blank and S. D. Minteer, *Chem. Rev.*, 2021, **122**, 3180–3218.
17 J. E. Kim, S. Choi, M. Balamurugan, J. H. Jang and K. T. Nam, *Trends Chem.*, 2020, **2**, 1004–1019.
18 J. Li, Y. Zhang, K. Kuruvinashetti and N. Kornienko, *Nat. Rev. Chem.*, 2022, **6**, 303–319.
19 D. Chen, J. Liu, J. Shen, Y. Zhang, H. Shao, C. Chen and S. Wang, *Adv. Energy Mater.*, 2024, **14**, 2303820.
20 T. L. Lohr and T. J. Marks, *Nat. Chem.*, 2015, **7**, 477–482.
21 X. Wang and R. Rinaldi, *Angew. Chem., Int. Ed.*, 2013, **52**, 11499–11503.
22 A. C. Atesin, N. A. Ray, P. C. Stair and T. J. Marks, *J. Am. Chem. Soc.*, 2012, **134**, 14682–14685.
23 K. E. Metzger, M. M. Moyer and B. G. Trewyn, *ACS Catal.*, 2020, **11**, 110–122.
24 F. Zaera, *Chem. Rev.*, 2022, **122**, 8594–8757.
25 M. J. Climent, A. Corma and S. Iborra, *Chem. Rev.*, 2011, **111**, 1072–1133.
26 T. Fukushima and M. Yamauchi, *Chem. Commun.*, 2019, **55**, 14721–14724.
27 T. Fukushima and M. Yamauchi, *J. Appl. Electrochem.*, 2021, **51**, 99–106.
28 E. Schuler, M. Demetriou, N. R. Shiju and G. J. M. Gruter, *ChemSusChem*, 2021, **14**, 3636–3664.
29 P. S. Lakkaraju, M. Askerka, H. Beyer, C. T. Ryan, T. Dobbins, C. Bennett, J. J. Kaczur and V. S. Batista, *ChemCatChem*, 2016, **8**, 3453–3457.
30 G. Hayes, M. Laurel, D. MacKinnon, T. Zhao, H. A. Houck and C. R. Becer, *Chem. Rev.*, 2022, **123**, 2609–2734.
31 Y. Ma, Y. Zhang, W. Yuan, M. Du, S. Kang and B. Qiu, *EES. Catal.*, 2023, 892–920.
32 J. E. Kim, J. H. Jang, K. M. Lee, M. Balamurugan, Y. I. Jo, M. Y. Lee, S. Choi, S. W. Im and K. T. Nam, *Angew. Chem., Int. Ed.*, 2021, **133**, 22114–22122.
33 Y. Cheng, S. Liu, J. Jiao, M. Zhou, Y. Wang, X. Xing, Z. Chen, X. Sun, Q. Zhu and Q. Qian, *J. Am. Chem. Soc.*, 2024, **146**, 10084–10092.
34 M. Sadakiyo, S. Hata, T. Fukushima, G. Juhász and M. Yamauchi, *Phys. Chem. Chem. Phys.*, 2019, **21**, 5882–5889.
35 J. Tafel and G. Friedrichs, *Ber. Dtsch. Chem. Ges.*, 1904, **37**, 3187–3191.
36 F. Goodridge, K. Lister, R. E. Plimley and K. Scott, *J. Appl. Electrochem.*, 1980, **10**, 55–60.
37 K. Scott, *Electrochim. Acta*, 1991, **36**, 1447–1452.
38 F. Go, *J. Appl. Electrochem.*, 1980, **10**, 55–60.
39 K. Scott, *Chem. Eng. Res. Des.*, 1986, **64**, 266–272.
40 I. Ivanov, Y. Stefanov, Z. Noncheva, M. Petrova, T. Dobrev, L. Mirkova, R. Vermeersch and J.-P. Demaerel, *Hydrometallurgy*, 2000, **57**, 109–124.
41 Y. Izumi, I. Chibata and T. Itoh, *Angew. Chem., Int. Ed. Engl.*, 1978, **17**, 176–183.
42 H. Gröger, *Chem. Rev.*, 2003, **103**, 2795–2828.
43 R. J. Block, *Chem. Rev.*, 1946, **38**, 501–571.
44 J. Xian, S. Li, H. Su, P. Liao, S. Wang, R. Xiang, Y. Zhang, Q. Liu and G. Li, *Angew. Chem., Int. Ed.*, 2023, e202306726.
45 K. Yan, M. L. Huddleston, B. A. Gerdes and Y. Sun, *Green Chem.*, 2022, **24**, 5320–5325.
46 M. Li, Y. Wu, B.-H. Zhao, C. Cheng, J. Zhao, C. Liu and B. Zhang, *Nat. Catal.*, 2023, **6**, 906–915.
47 J. Xian, S. Li, H. Su, P. Liao, S. Wang, Y. Zhang, W. Yang, J. Yang, Y. Sun and Y. Jia, *Angew. Chem., Int. Ed.*, 2023, **62**, e202304007.
48 Y. Xiao, C. W. Lim, J. Chang, Q. Yuan, L. Wang and N. Yan, *Green Chem.*, 2023, **25**, 3117–3126.
49 P. J. Broersen, T. de Groot, D. F. Bruggeman, E. S. Caarls, J. A. Trindell, D. Anastasiadou, M. C. Figueiredo, G. Rothenberg and A. C. Garcia, *ChemCatChem*, 2024, **16**, e202301370.
50 L. Li, C. Wan, S. Wang, X. Li, Y. Sun and Y. Xie, *Nano Lett.*, 2024, 2392–2399.
51 P. Li, K. Wang and B. Zhang, *ACS Appl. Mater. Interfaces*, 2024, **16**, 57171–57179.
52 K. Wang, P. Li and B. Zhang, *Appl. Catal., B*, 2025, **361**, 124653.